

# Recombination Kinetics and Effects of Superacid Treatment in Sulfur- and Selenium-Based Transition Metal Dichalcogenides

Matin Amani,<sup>†,‡</sup> Peyman Taheri,<sup>†</sup> Rafik Addou,<sup>§</sup> Geun Ho Ahn,<sup>†,‡</sup> Daisuke Kiriya,<sup>†,‡</sup> Der-Hsien Lien,<sup>†,‡</sup> Joel W. Ager, III,<sup>‡</sup> Robert M. Wallace,<sup>§</sup> and Ali Javey<sup>\*,†,‡</sup>

<sup>†</sup>Electrical Engineering and Computer Sciences, University of California, Berkeley, California 94720, United States

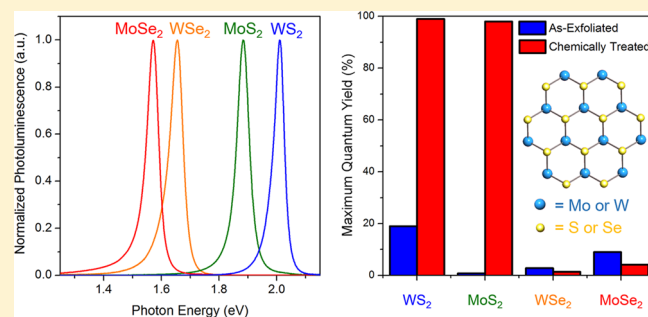
<sup>‡</sup>Materials Sciences Division, Lawrence Berkeley National Laboratory, Berkeley, California 94720, United States

<sup>§</sup>Department of Materials Science and Engineering, University of Texas, Dallas, Richardson, Texas 75080, United States

## Supporting Information

**ABSTRACT:** Optoelectronic devices based on two-dimensional (2D) materials have shown tremendous promise over the past few years; however, there are still numerous challenges that need to be overcome to enable their application in devices. These include improving their poor photoluminescence (PL) quantum yield (QY) as well as better understanding of exciton-based recombination kinetics. Recently, we developed a chemical treatment technique using an organic superacid, bis(trifluoromethane)sulfonimide (TFSI), which was shown to improve the quantum yield in MoS<sub>2</sub> from less than 1% to over 95%. Here, we perform detailed steady-state and transient optical characterization on some of the most heavily studied direct bandgap 2D materials, specifically WS<sub>2</sub>, MoS<sub>2</sub>, WSe<sub>2</sub>, and MoSe<sub>2</sub>, over a large pump dynamic range to study the recombination mechanisms present in these materials. We then explore the effects of TFSI treatment on the PL QY and recombination kinetics for each case. Our results suggest that sulfur-based 2D materials are amenable to repair/passivation by TFSI, while the mechanism is thus far ineffective on selenium based systems. We also show that biexcitonic recombination is the dominant nonradiative pathway in these materials and that the kinetics for TFSI treated MoS<sub>2</sub> and WS<sub>2</sub> can be described using a simple two parameter model.

**KEYWORDS:** Transition metal dichalcogenide, quantum yield, radiative lifetime, biexcitonic recombination



Monolayer optoelectronics has been a rapidly growing field since the isolation of graphene<sup>1–3</sup> and has received intensified interest after the identification of direct-bandgap monolayers, starting with MoS<sub>2</sub><sup>4</sup> as well as other two-dimensional (2D) transition metal dichalcogenides (TMDCs).<sup>5,6</sup> At the monolayer limit, numerous new phenomena are observed in these materials such as the presence of valley and spin-based physics,<sup>7–9</sup> which can enable new device paradigms. Furthermore, they possess several advantages over conventional optically active materials such as the ability to form heterostructures without the need for lattice matching,<sup>10</sup> exceptional tunability via electric field or strain,<sup>11,12</sup> and high absorption given their atomic scale thickness.<sup>5</sup> One of the main challenges for two-dimensional optoelectronics, however, is their poor photoluminescence (PL) quantum yields (QY),<sup>5</sup> which is the key metric for all optoelectronic devices, including lasers, LEDs, and solar cells.<sup>13,14</sup> Furthermore, PL QY is an extremely sensitive probe of defects and sub-bandgap states and thus semiconductor quality,<sup>15</sup> as such it can serve as a metric to determine the viability of a material for device applications such as tunnel transistors.<sup>16</sup>

Unlike conventional 3D materials, where terminations in the crystal lattice result in dangling bonds, ideal 2D systems have natural out-of-plane self-termination. As a result, it could be expected that monolayer semiconductors should show near-unity PL QY, whereas materials such as GaAs require cladding layers (i.e., AlGaAs) to show similar performance.<sup>17,18</sup> However, due to the presence of defects, the QY in 2D materials has typically been quite poor.<sup>5</sup> Fortunately, monolayer semiconductors also offer a unique opportunity for defect passivation/repair because there is no distinction between bulk and surface defects, as such the entire semiconductor can be accessed. In our previous work, we demonstrated that PL QY in MoS<sub>2</sub> monolayers on oxide substrates can be dramatically enhanced through chemical treatment by the nonoxidizing organic superacid, bis(trifluoromethane)sulfonimide (TFSI), resulting in the realization of near-unity QY.<sup>19</sup> Recently, other chemical treatments have also been developed which are able to enhance the PL of

**Received:** February 6, 2016

**Revised:** March 8, 2016

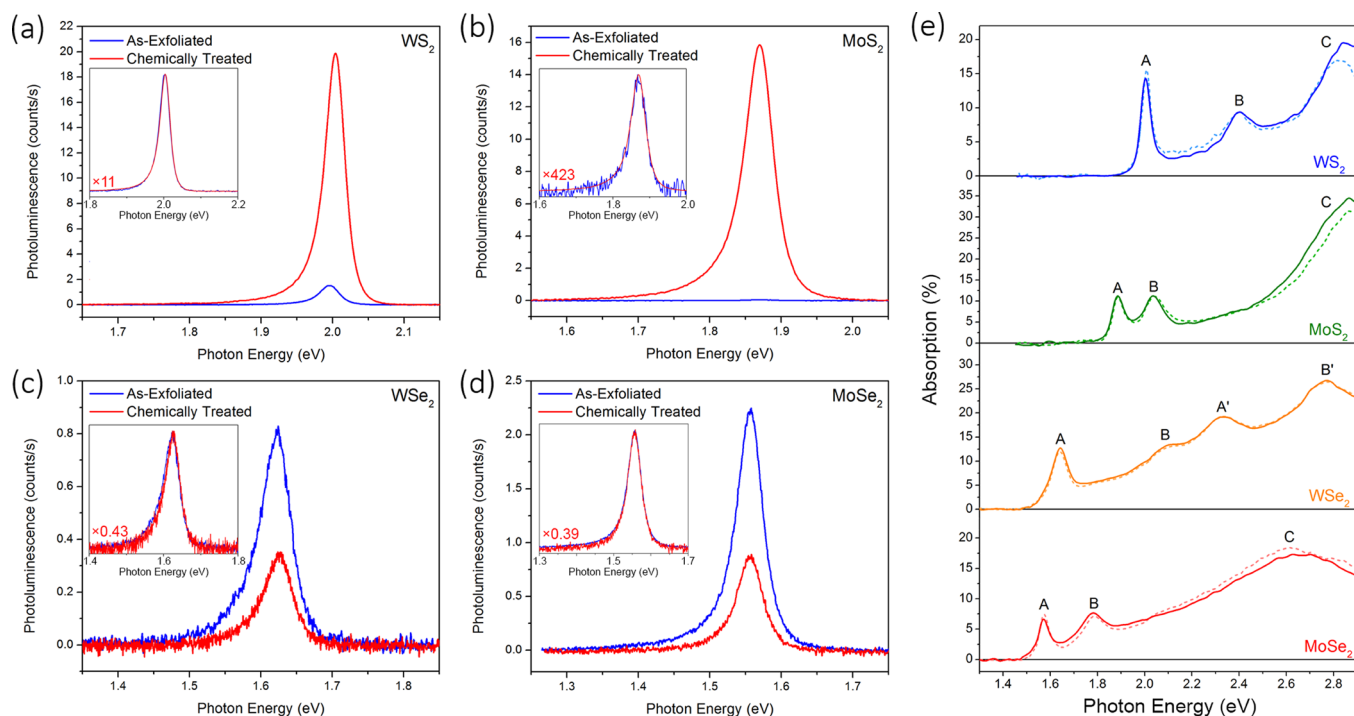


**Figure 1.** PL spectra for both the as-exfoliated and TFSI treated (a)  $\text{WS}_2$ , (b)  $\text{MoS}_2$ , (c)  $\text{WSe}_2$ , and (d)  $\text{MoSe}_2$  monolayers measured at an incident power density of  $1 \times 10^{-2} \text{ W cm}^{-2}$ . The inset shows normalized spectra for each material. Absorption spectra of both as-exfoliated (dashed lines) and chemically treated (solid lines)  $\text{WS}_2$ ,  $\text{MoS}_2$ ,  $\text{WSe}_2$ , and  $\text{MoSe}_2$  monolayers (e).

$\text{MoS}_2$ <sup>20</sup> and  $\text{MoSe}_2$ .<sup>21</sup> Here, we expand on upon the initial results by studying the effect of TFSI treatment in combination with combined steady-state and transient optical measurements, on several of the most optoelectronically promising TMDC monolayers<sup>5,6</sup> including  $\text{WS}_2$ ,  $\text{WSe}_2$ , and  $\text{MoSe}_2$ . We find that the treatment is able to effectively passivate/repair defects in sulfur based compounds, while the selenide-based materials are largely unaffected. Furthermore, we observe that all of these materials display similar recombination kinetics, that is, there is no observable Shockley–Read–Hall (SRH) recombination at low injection levels while biexcitonic recombination dominates at high injection levels.

To verify that treatment by TFSI does not damage the 2D compounds investigated in this study, we performed Raman spectroscopy for each material studied both in the as-exfoliated case and after TFSI treatment, as illustrated in Figure S1a–d. The Raman spectra of  $\text{WS}_2$  under 514.5 nm excitation is a particularly interesting case, because under this condition there is a second order-resonance with the longitudinal acoustic mode (LA(M)) that is a result of coupling between the phonon and electronic band structures.<sup>22</sup> While there is no significant change in the Raman spectra for  $\text{WSe}_2$  or  $\text{MoSe}_2$  after chemical treatment, both in terms of peak position and relative intensity, as was observed for  $\text{MoS}_2$  in our previous report,<sup>19</sup> we observe a strong increase in the intensity ratio of the 2LA(M) peak to the A' peak from 2.9, which is comparable to what has been previously observed for  $\text{WS}_2$  monolayers,<sup>22,23</sup> to 5.3. The increased relative intensity of the resonant mode suggests that the influence of defects is reduced after chemical treatment. Furthermore, this trend is consistent with reduced 2LA(M)/A' peak intensity recently observed for lower quality  $\text{WS}_2$  samples.<sup>23</sup>

Steady-state calibrated PL spectra, measured at a low excitation power density of  $1 \times 10^{-2} \text{ W cm}^{-2}$  for the four

materials examined in this study, are shown in Figure 1a–d. Normalized spectra indicate that TFSI treatment does not result in any shifts or significant changes in the spectral line shape at low excitation densities. We found that in addition to being able to dramatically enhance the PL of  $\text{MoS}_2$ , TFSI treatment is also effective in repairing/passivating defects in  $\text{WS}_2$ . As-exfoliated  $\text{WS}_2$  has been known to show the highest quantum yield of all 2D materials, which have been previously studied;<sup>24,25</sup> despite this, we are still able to demonstrate an order of magnitude enhancement of the emission, relative to the as-exfoliated monolayer. To be able to extract the internal photoluminescence quantum yield for the different samples quantitative absorption measurements were performed for each system both before and after chemical treatment. The measurements were performed using two different methods, following the procedure described in our previous work, and are plotted in Figure 1e. As was previously shown for  $\text{MoS}_2$ , there is no measurable difference in the absorption spectra as a result of TFSI treatment in  $\text{WS}_2$ ,  $\text{WSe}_2$ , or  $\text{MoSe}_2$ . The spectral shape of the calibrated absorption spectra presented here is consistent with previously reported differential reflectance measurements on the various materials.<sup>26</sup>

One of the primary factors that affects the observed luminescence in 2D semiconductors is substrate-induced interference and multiple reflection effects.<sup>27</sup> These phenomena can modulate both the effective absorption as well as the emission by increasing the number of times an incident or emitted photon can be absorbed by the 2D layer or the number of chances it has to fall within the escape cone for emission. By changing the oxide thickness on silicon substrates, it was previously shown that this effect can lead to an order of magnitude modulation in the emitted light for the same monolayer,<sup>27</sup> indicating that this effect is independent of the materials internal PL QY. More importantly, this effect has

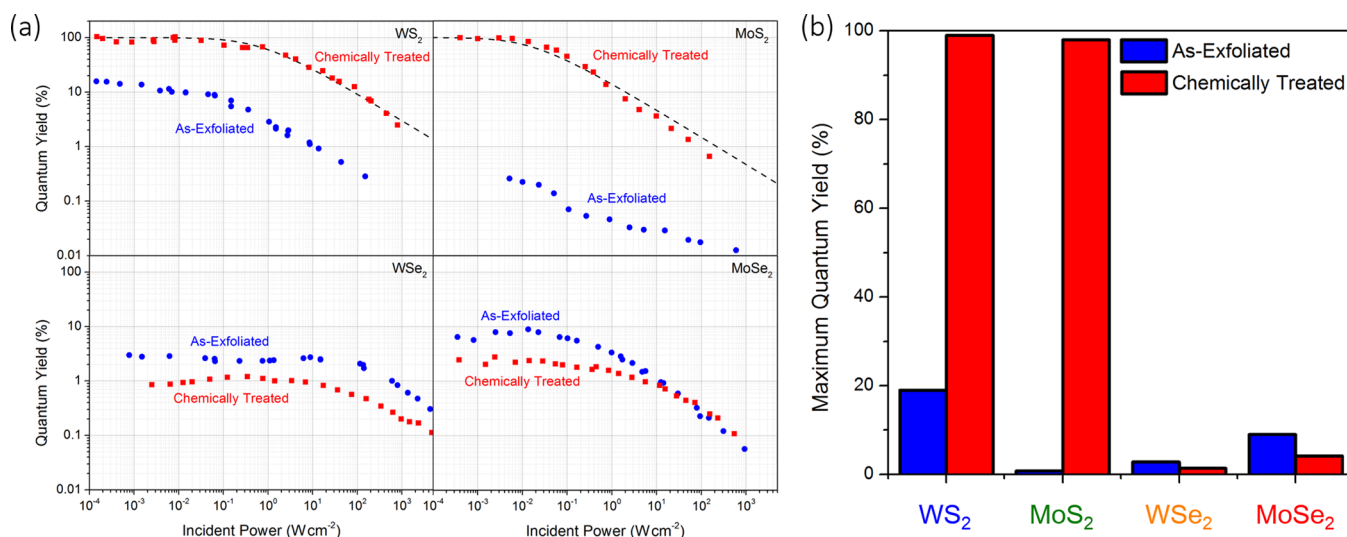


**Figure 2.** Pump-power dependence of the QY for as-exfoliated and chemically treated WS<sub>2</sub>, MoS<sub>2</sub>, WSe<sub>2</sub>, and MoSe<sub>2</sub> (a). Dashed lines show the recombination model for chemically treated MoS<sub>2</sub> and WS<sub>2</sub>. Summary of the peak QY values for the various TMDCs obtained both before and after treatment (b).

significant wavelength dependence and will nonlinearly weight the observed luminescence for different light emitters. In the case of GaAs, by placing the sample on a highly reflective mirror substrate, it is possible to dramatically increase the probability of the emitted light escaping to  $\sim 70\%$ .<sup>17</sup> In addition, complex optical environments such as Si/SiO<sub>2</sub> can impact the radiative lifetime through changes in the effective refractive index.<sup>28</sup> For our case, we utilized quartz substrates for all measurements, which provides a very simple, nonwavelength dependent analysis, although this lowers the externally measured luminescence.

To probe the recombination mechanisms present in the various TMDCs, we extended our PL measurements to cover a pump dynamic range of over 6 orders of magnitude, while avoiding incident laser powers greater than 50  $\mu\text{W}$  that are known to damage as well as cause local heating effects in these materials.<sup>29</sup> The pump-power dependence of luminescence for the different materials is shown both before and after chemical treatment in Figure S2, as well as empirical power law fits, given by  $I = P^n$ , to the dominant recombination regimes. From these curves we extract the QY, which is plotted in Figure 2 for each material both before and after treatment. After treatment, the QY for both MoS<sub>2</sub> and WS<sub>2</sub> reaches a value near-unity at low pump power, while the QY for the two selenide materials is moderately reduced as summarized in Figure 2b. At high injection levels all of the investigated materials show sublinear dependence of the light emission with rate-laws in the range of 0.43–0.58. The rate law is indicative of a two-body nonradiative process and can be attributed to biexcitonic recombination (annihilation of two excitons), knowing that free electron–hole pairs in 2D materials nonreversibly form excitons due to their high binding energies.<sup>30</sup> In all cases, as the excitation power is reduced, the materials show saturation of the PL, that is, no reduction of the luminescence yield. This is strongly in contrast with traditional semiconductors where a reduction of the PL QY is typically observed due to SRH recombination of a carrier at a defect site (one body process) as opposed to meeting an oppositely charged carrier and radiating (two body process).<sup>31</sup> For the excitonic case, both recombination with a defect and

radiation are single body processes that leads to the observed luminescence saturation.

The dynamic luminescence behavior for the different materials, both in the as-exfoliated and chemically treated cases, was investigated to examine the carrier recombination dynamics as well as independently confirm the QY measurements. We show the decay curves for as-exfoliated and chemically treated WS<sub>2</sub> in Figure 3 panels a and b, respectively, and the lifetime for both cases as a function of pump-fluence is shown in Figure 3c and is consistent with the behavior observed in the steady-state measurements. Chemically treated WS<sub>2</sub> shows a single exponential decay with a radiative lifetime ( $\tau_r$ ) of  $3.4 \pm 0.3$  ns as the lowest measured fluence of  $2.3 \times 10^{-4}$   $\mu\text{J}/\text{cm}^2$ . Similar measurements were performed on WSe<sub>2</sub> and MoSe<sub>2</sub> and are shown in Figure S5. Figure 3d summarizes the observed lifetimes ( $\tau_{\text{ob}}$ ) for the materials evaluated in this study. Although the luminescence decay of the selenide compounds is dominated by the nonradiative lifetime, we can estimate the radiative lifetime using<sup>31</sup>

$$QY = \frac{\tau_{\text{ob}}}{\tau_r}$$

which results in  $\tau_r = 19.3$  ns and  $\tau_r = 116.3$  ns for WSe<sub>2</sub> and MoSe<sub>2</sub>, respectively.

The carrier density-dependent recombination mechanisms for TFSI treated WS<sub>2</sub> and MoS<sub>2</sub> can be effectively described using the kinetic model that we previously proposed for exciton dominated semiconductors.<sup>19</sup> This differs from the free carrier model used to describe III–V semiconductors that is based solely on free carriers due to their negligible exciton binding energies at room temperature. For the free carrier approach, at low background doping concentrations where the majority of free-carriers are generated by optical pumping  $n = p$ , where  $n$  and  $p$  are the electron and hole concentrations, respectively. For this case, at steady state the total recombination rate  $R$  is equal to the generation rate and can be written as  $R = An + Bn^2 + Cn^3$ , where  $A$  is the SRH recombination rate,  $B$  is the radiative recombination rate,  $C$  is the Auger recombination rate, and QY is given as the ratio of radiative recombination over total recombination.<sup>31</sup> Auger processes dominate at high

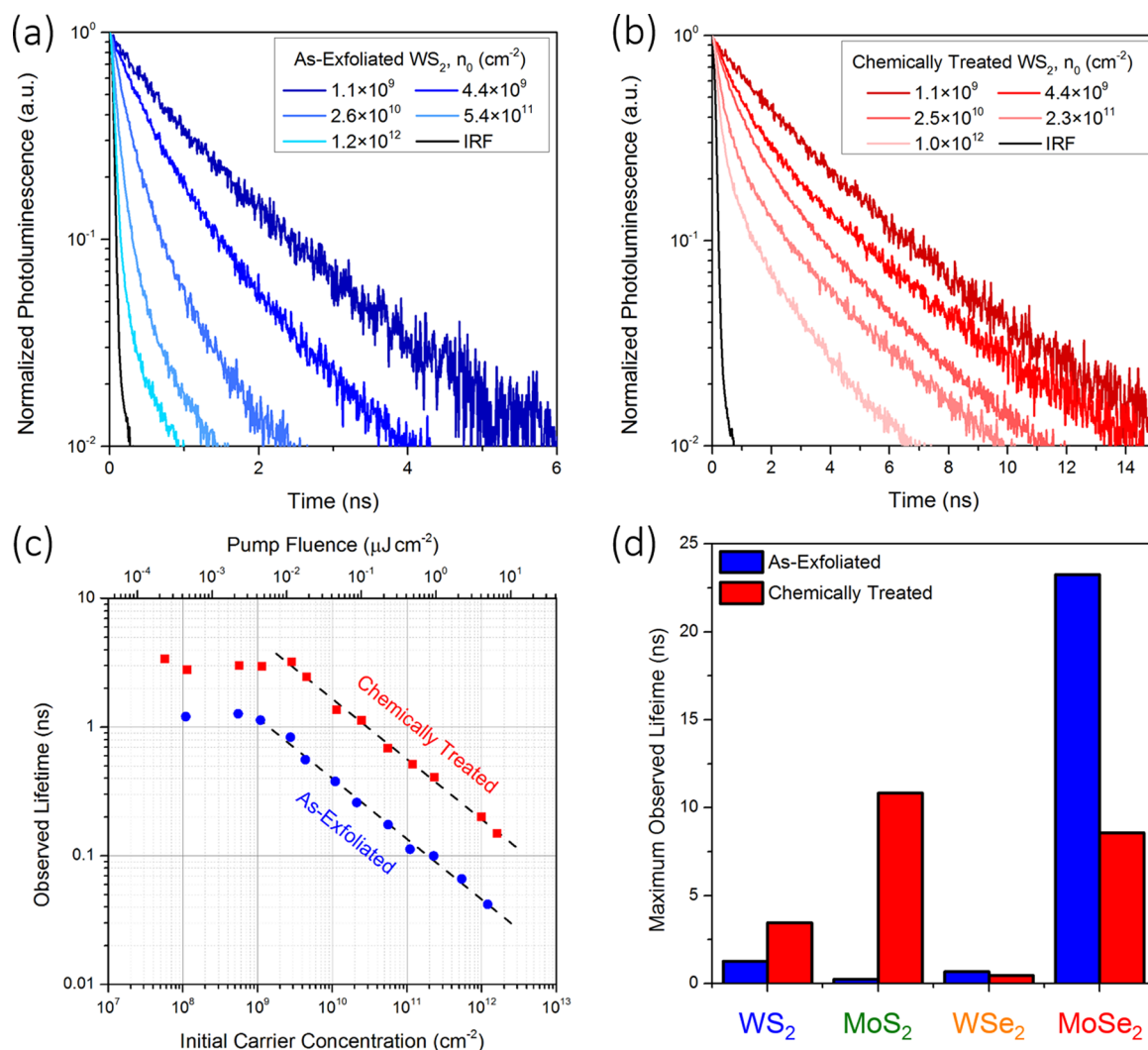


**Figure 3.** Radiative decay of as-exfoliated (a) and chemically treated (b) WS<sub>2</sub> at various initial carrier concentrations ( $n_0$ ) as well as the instrument response function (IRF). Effective PL lifetime as a function of pump-fluence for WS<sub>2</sub> both before and after chemical treatment; the dashed line shows a power law fit for the dominant recombination regimes (c). Summary of longest measured lifetimes for the various TMDCs obtained both before and after treatment (d); lifetime measurements before and after treatment are shown in Figure S5.

injection levels, while SRH recombination dominates at low injection levels. For the case of SRH dominated recombination, the QY increases as a function of pump-power, which was not observed for any of the studied TMDCs.

Because the standard model was found to poorly describe the data both here and in our initial work,<sup>19</sup> we utilized a simple model based on the total exciton population,  $\langle N \rangle$ . In this interpretation, the dominant intrinsic nonradiative recombination method occurs from the collision of two excitons and is proportional to  $\langle N \rangle^2$ . Total recombination of free carriers is set to  $R = B_{nr}n^2 + B_r n^2$ . Here,  $B_{nr}$  is the nonradiative defect-mediated recombination rate and  $B_r$  is the formation rate of excitons. It is likely that there are multiple nonradiative pathways possible due to the diverse nature of defects present in 2D materials,<sup>32,33</sup> and the role of the various optoelectronically active defects in recombination must be evaluated using controlled techniques to fully understand their behavior. For the purpose of the present work, we only consider the cases of TFSI treated WS<sub>2</sub> and MoS<sub>2</sub> that show no nonradiative pathways at low excitation levels. In this case, excitons can then undergo radiative recombination or nonradiatively recombine with a second exciton, which is given by  $B_r n^2 = \tau_r^{-1} \langle N \rangle +$

$C_{bx} \langle N \rangle^2$ , where  $\tau_r$  is the radiative lifetime and  $C_{bx}$  is the biexcitonic recombination rate. The final QY is then given as

$$QY = \frac{\tau_r^{-1} \langle N \rangle}{\tau_r^{-1} \langle N \rangle + B_{nr} n^2 + C_{bx} \langle N \rangle^2}$$

For TFSI-treated MoS<sub>2</sub> and WS<sub>2</sub>,  $B_{nr}$  is negligible, resulting in a biexcitonic recombination coefficient of 0.5 and 2.8 cm<sup>2</sup> s<sup>-1</sup>, respectively. The fitting results for both cases are plotted as dashed lines in Figure 2a. The specific value of the biexcitonic recombination coefficient for WS<sub>2</sub> and MoS<sub>2</sub> was found to be highly reproducible among different samples as shown in Figures S3 and S4, suggesting that it is an intrinsic material parameter.

The 2D materials are known to be host to a significant variety of defect types<sup>23,32–35</sup> in naturally or synthesized crystals as well as monolayers grown by chemical vapor deposition.<sup>36</sup> In the case of both exfoliated WS<sub>2</sub> and MoS<sub>2</sub>, which can achieve near-unity QY after TFSI treatment, one of the dominant defect types is likely sulfur vacancies.<sup>26,34</sup> On the other hand, TFSI treatment is not able to improve the luminescence of both WSe<sub>2</sub> and MoSe<sub>2</sub> and typically results in a

small drop from the as-exfoliated intensity. The treatment conditions for the selenium-based compounds were systematically varied, as discussed further in the [Supporting Information](#), however no TFSI-based treatment condition was found to enhance the PL. High-resolution TEM studies on  $\text{WSe}_2$  have suggested that defects in this material do not simply exist as simple vacancy sites but rather as complexes that include both missing chalcogen and metal atoms.<sup>33</sup>

To better understand the nature of the native defects that exist in the various crystals, scanning tunneling microscopy (STM) measurements were performed on freshly exfoliated crystals of the materials studied here. Representative STM images taken over a similar area of  $100 \text{ nm} \times 100 \text{ nm}$  for the different TMDC materials are shown in [Figure 4](#); it is

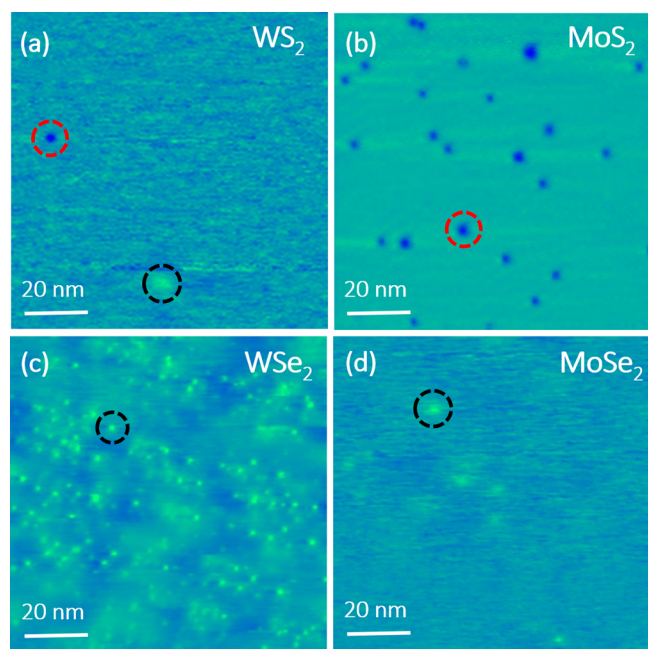


**Figure 4.** Large area representative STM images ( $100 \text{ nm} \times 100 \text{ nm}$ ) measured on bulk flakes of (a)  $\text{WS}_2$  ( $V_{\text{bias}} = 0.9 \text{ V}$ ,  $I_t = 1.0 \text{ nA}$ ), (b)  $\text{MoS}_2$  ( $V_{\text{bias}} = 1.0 \text{ V}$ ,  $I_t = 1.0 \text{ nA}$ ), (c)  $\text{WSe}_2$  ( $V_{\text{bias}} = 1.5 \text{ V}$ ,  $I_t = 0.5 \text{ nA}$ ), and (d)  $\text{MoSe}_2$  ( $V_{\text{bias}} = 1.5 \text{ V}$ ,  $I_t = 0.5 \text{ nA}$ ). Red circles show examples of either donor impurities or missing fragments of material (dark contrast); black circles indicate show examples of acceptor impurities (bright contrast).

important to note here that the spatial variation of surface defects is high. The poor QY observed in as-exfoliated  $\text{MoS}_2$  can be understood from the comparatively large defect density observed in STM (as high as 8% of the imaged surface area), relative to  $\text{WS}_2$  ( $\sim 0.1\text{--}1.6\%$ ). Dark contrast defects, predominantly observed in  $\text{WS}_2$  and  $\text{MoS}_2$ , can be caused by missing fragments of the material as well as the presence of acceptor impurities at the vicinity of the surface region.<sup>36–38</sup> This is consistent with sulfur vacancies and the n-type behavior observed in  $\text{WS}_2$  and  $\text{MoS}_2$  field effect devices,<sup>35,39</sup> which do not utilize doping or extremely high work function contacts to enable p-type conduction.<sup>40,41</sup> The opposite behavior is seen in selenides where a high density of bright contrast defects ( $>2\%$ ) that can primarily be related to donor impurities at or near the surface are observed.<sup>42</sup> The interpretation of the localized imperfections were well documented for GaAs(110) and other semiconductors.<sup>43</sup> Our surface inspection reveals the following findings: (i) high spatial variation even across the same material

with the largest imperfection density found on  $\text{MoS}_2$ , (ii) sulfide surfaces are dominated by structural defects and by acceptor impurities causing local depressions, and (iii) selenide surfaces are predominantly dominated by hillock-like structures induced by donor impurities. This drastic difference in the nature of defects may explain why sulfur-based TMDC materials are more responsive to the TFSI treatment.

In summary, we have presented a comprehensive study on the recombination behavior as well as the impact of TFSI treatment on the most heavily studied direct band gap 2D semiconductors. We show that the dominant recombination pathway at high pump-power for all of these materials is biexcitonic recombination and that there is no evidence for SRH-related recombination at low injection levels. Furthermore, through the combination of lifetime and calibrated QY measurements we estimate the radiative lifetimes and provide the biexcitonic recombination coefficients for the studied systems. Our results show that sulfur-based TMDCs are amenable to repair by TFSI treatment, while high QY in selenium-based compounds cannot be obtained by this method.

## ■ ASSOCIATED CONTENT

### 📄 Supporting Information

The Supporting Information is available free of charge on the ACS Publications website at DOI: [10.1021/acs.nanolett.6b00536](https://doi.org/10.1021/acs.nanolett.6b00536).

Materials and methods, Raman spectra, pump-power dependence of PL, QY measurements on additional samples, and time-resolved luminescence measurements. (PDF)

## ■ AUTHOR INFORMATION

### Corresponding Author

\*E-mail: [ajavey@berkeley.edu](mailto:ajavey@berkeley.edu).

### Author Contributions

The manuscript was written through contributions of all authors. All authors have given approval to the final version of the manuscript.

### Funding

This work was supported by the Electronic Materials Program, funded by Director, Office of Science, Office of Basic Energy Sciences, Materials Sciences and Engineering Division of the U.S. Department of Energy under Contract No. DE-AC02-05Ch11231. P.T. was supported by a fellowship awarded by NWO-Rubicon. R.A. and R.M.W. were funded by the Center for Low Energy Systems Technology (LEAST), one of six centers supported by the STARnet phase of the Focus Center Research Program (FCRP), a Semiconductor Research Corporation program sponsored by MARCO and DARPA and by the Southwest Academy on Nanoelectronics (SWAN) sponsored by the Nanoelectronic Research Initiative (NRI) and NIST.

### Notes

The authors declare no competing financial interest.

## ■ REFERENCES

- (1) Bonaccorso, F.; Sun, Z.; Hasan, T.; Ferrari, A. C. *Nat. Photonics* **2010**, *4*, 611–622.
- (2) Mueller, T.; Xia, F.; Avouris, P. *Nat. Photonics* **2010**, *4*, 297–301.
- (3) Liu, M.; Yin, X.; Ulin-Avila, E.; Geng, B.; Zentgraf, T.; Ju, L.; Wang, F.; Zhang, X. *Nature* **2011**, *474*, 64–67.

- (4) Mak, K. F.; Lee, C.; Hone, J.; Shan, J.; Heinz, T. F. *Phys. Rev. Lett.* **2010**, *105*, 136805.
- (5) Zhao, W.; Ghorannevis, Z.; Chu, L.; Toh, M.; Kloc, C.; Tan, P.-H.; Eda, G. *ACS Nano* **2013**, *7* (1), 791–797.
- (6) Lezama, I. G.; Arora, A.; Ubaldini, A.; Barreateau, C.; Giannini, E.; Potemski, M.; Morpurgo, A. F. *Nano Lett.* **2015**, *15* (4), 2336–2342.
- (7) Mak, K. F.; He, K.; Shan, J.; Heinz, T. F. *Nat. Nanotechnol.* **2012**, *7*, 494–498.
- (8) Xiao, D.; Liu, G. B.; Feng, W.; Xu, X.; Yao, W. *Phys. Rev. Lett.* **2012**, *108*, 196802.
- (9) Zeng, H.; Dai, J.; Yao, W.; Xiao, D.; Cui, X. *Nat. Nanotechnol.* **2012**, *7*, 490–493.
- (10) Fang, H.; Battaglia, C.; Carraro, C.; Nemsak, S.; Ozdol, B.; Kang, J. S.; Bechtel, H. A.; Desai, S. B.; Kronast, F.; Unal, A. A.; Conti, G.; Conlon, C.; Palsson, G. K.; Martin, M. C.; Minor, A. M.; Fadley, C. S.; Yablonovitch, E.; Maboudian, R.; Javey, A. *Proc. Natl. Acad. Sci. U. S. A.* **2014**, *111* (17), 6198–6202.
- (11) Ramasubramaniam, A.; Naveh, D.; Towe, E. *Phys. Rev. B: Condens. Matter Mater. Phys.* **2011**, *84*, 205325.
- (12) Desai, S. B.; Seol, G.; Kang, J. S.; Fang, H.; Battaglia, C.; Kapadia, R.; Ager, J. W.; Guo, J.; Javey, A. *Nano Lett.* **2014**, *14*, 4592–4597.
- (13) Miller, O. D.; Yablonovitch, E.; Kurtz, S. R. *IEEE J. Photovolt.* **2012**, *2* (3), 303–311.
- (14) Sutter-Fella, C. M.; Li, Y.; Amani, M.; Ager, J. W.; Toma, F. M.; Yablonovitch, E.; Sharp, I. D.; Javey, A. *Nano Lett.* **2016**, *16* (1), 800–806.
- (15) Trupke, T.; Bardos, R. A.; Schubert, M. C.; Warta, W. *Appl. Phys. Lett.* **2006**, *89*, 044107.
- (16) Ionescu, A. M.; Riel, H. *Nature* **2011**, *479*, 329–337.
- (17) Schnitzer, I.; Yablonovitch, E.; Caneau, C.; Gmitter, T. J. *Appl. Phys. Lett.* **1993**, *62*, 131–133.
- (18) Guidotti, D.; Hasan, E.; Hovel, H. J.; Albert, M. *Appl. Phys. Lett.* **1987**, *50*, 912–914.
- (19) Amani, M.; Lien, D.-H.; Kiriya, D.; Xiao, J.; Azcatl, A.; Noh, J.; Madhvapathy, S. R.; Addou, R.; Kc, S.; Dubey, M.; Cho, K.; Wallace, R. M.; Lee, S.-C.; He, J.-H.; Ager, J. W.; Zhang, X.; Yablonovitch, E.; Javey, A. *Science* **2015**, *350*, 1065–1068.
- (20) Su, W.; Dou, H.; Li, J.; Huo, D.; Dai, N.; Yang, Li. *RSC Adv.* **2015**, *5*, 82924.
- (21) Han, H.-V.; Lu, A.-Y.; Lu, L.-S.; Huang, J.-K.; Li, H.; Hsu, C.-L.; Lin, Y.-C.; Chiu, M.-H.; Suenaga, K.; Chu, C.-W.; Kuo, H.-C.; Chang, W.-H.; Li, L.-J.; Shi, Y. *ACS Nano* **2016**, *10* (1), 1454–1461.
- (22) Berkdemir, A.; Gutierrez, H. R.; Botello-Mendez, A. R.; Perea-Lopez, N.; Elias, A. L.; Chia, C. I.; Wang, B.; Crespi, V. H.; Lopez-Urias, F.; Charlier, J. C.; Terrones, H.; Terrones, M. *Sci. Rep.* **2013**, *3*, 1755.
- (23) McCreary, A.; Berkdemir, A.; Wang, J.; Nguyen, M. A.; Elias, A. L.; Perea-Lopez, N.; Fujisawa, K.; Kabius, B.; Carozo, V.; Cullen, D. A.; Mallouk, T. E.; Zhu, J.; Terrones, M. *J. Matter. Res.* **2016**, DOI: 10.1557/jmr.2016.47, in press.
- (24) Yuan, L.; Huang, L. *Nanoscale* **2015**, *7*, 7402.
- (25) Gutierrez, H. R.; Perea-Lopez, N.; Elias, A. L.; Berkdemir, A.; Wang, B.; Lv, R.; Lopez-Urias, F.; Crespi, V. H.; Terrones, H.; Terrones, M. *Nano Lett.* **2013**, *13* (8), 3447–3454.
- (26) Kozawa, D.; Kumar, R.; Carvalho, A.; Kumar Amara, K. K.; Zhao, W.; Wang, S.; Toh, M.; Ribeiro, R. M.; Castro Neto, A. H.; Matsuda, K.; Eda, G. *Nat. Commun.* **2014**, *5*, 4543.
- (27) Lien, D.-H.; Kang, J. S.; Amani, M.; Chen, K.; Tosun, M.; Wang, H.-P.; Roy, T.; Eggleston, M. S.; Wu, M. C.; Dubey, M.; Lee, S.-C.; He, J.-H.; Javey, A. *Nano Lett.* **2015**, *15* (2), 1356–1361.
- (28) Yablonovitch, E.; Gmitter, T. J.; Bhat, R. *Phys. Rev. Lett.* **1988**, *61* (22), 2546–2549.
- (29) Liu, Z.; Amani, M.; Najmaei, S.; Xu, Q.; Zou, X.; Zhou, W.; Yu, T.; Qiu, C.; Birdwell, A. G.; Crowne, F. J.; Vajtai, R.; Yakobson, B. I.; Xia, Z.; Dubey, M.; Ajayan, P. M.; Lou, J. *Nat. Commun.* **2014**, *5*, S246.
- (30) Hill, H. M.; Rigosi, A. F.; Roquelet, C.; Chernikov, A.; Berkelbach, T. C.; Reichman, D. R.; Hybertsen, M. S.; Brus, L. E.; Heinz, T. F. *Nano Lett.* **2015**, *15* (5), 2992–2997.
- (31) Pelant, I. and Valenta, J. *Luminescence Spectroscopy of Semiconductors*; Oxford University Press: Oxford, 2012.
- (32) Qiu, H.; Xu, Tao; Wang, Z.; Ren, W.; Nan, H.; Ni, Z.; Chen, Q.; Yuan, S.; Miao, F.; Song, F.; Long, G.; Shi, Y.; Sun, L.; Wang, J.; Wang, X. *Nat. Commun.* **2013**, *4*, 2642.
- (33) Lin, Y.-C.; Bjorkman, T.; Komsa, H.-P.; Teng, P.-Y.; Yeh, C.-H.; Huang, F.-S.; Lin, K.-H.; Jadcak, J.; Huang, Y.-S.; Chiu, P.-W.; Krashennnikov, A. V.; Suenaga, K. *Nat. Commun.* **2015**, *6*, 6736.
- (34) Hong, J.; Hu, Z.; Probert, M.; Li, K.; Lv, D.; Yang, X.; Gu, L.; Mao, N.; Feng, Q.; Xie, L.; Zhang, J.; Wu, D.; Zhang, Z.; Jin, C.; Ji, W.; Zhang, X.; Yuan, J.; Zhang, Z. *Nat. Commun.* **2015**, *6*, 6293.
- (35) Najmaei, S.; Liu, Z.; Zhou, W.; Zou, X.; Shi, G.; Lei, S.; Yakobson, B. I.; Idrobo, J.-C.; Ajayan, P. M.; Lou, J. *Nat. Mater.* **2013**, *12*, 754–759.
- (36) Addou, R.; McDonnell, S.; Barrera, Z.; Guo, Z.; Azcatl, A.; Wang, J.; Zhu, H.; Hinkle, C. L.; Quevedo-Lopez, M.; Alshareef, H. N.; Colombo, L.; Hsu, J. W. P.; Wallace, R. M. *ACS Nano* **2015**, *9*, 9124–9133.
- (37) Addou, R.; Colombo, L.; Wallace, R. M. *ACS Appl. Mater. Interfaces* **2015**, *7*, 11921–11929.
- (38) McDonnell, S.; Addou, R.; Buie, C.; Wallace, R. M.; Hinkle, C. L. *ACS Nano* **2014**, *8*, 2880–2888.
- (39) Ovchinnikov, D.; Allain, A.; Huang, Y.-S.; Dumcenco, D.; Kis, A. *ACS Nano* **2014**, *8* (8), 8174–8181.
- (40) Kiriya, D.; Zhou, Y.; Nelson, C.; Hettick, M.; Madhvapathy, S. R.; Chen, K.; Zhao, P.; Tosun, M.; Minor, A. M.; Chrzan, D. C.; Javey, A. *Adv. Funct. Mater.* **2015**, *25*, 6257–6264.
- (41) Chuang, S.; Battaglia, C.; Azcatl, A.; McDonnell, S.; Kang, J. S.; Yin, X.; Tosun, M.; Kapadia, R.; Fang, H.; Wallace, R. M.; Javey, A. *Nano Lett.* **2014**, *14*, 1337–1342.
- (42) Whangbo, M. H.; Ren, J.; Magonov, S. N.; Bengel, H.; Parkinson, B. A.; Suna, A. *Surf. Sci.* **1995**, *326*, 311–326.
- (43) Ebert, P. *Surf. Sci. Rep.* **1999**, *33*, 121–303.